Experimental method for the extraction of intensity profiles by imaging the scattered pattern with a charge-coupled device

Haixia Li (李海霞)[1,2], Meina Zhang (张美娜)[2], Xiaoyi Chen (陈小艺)[2], Chunxiang Liu (刘春香)[2], and Chuanfu Cheng (程传福)[2*]

[1] *Department of Information Science and Technology, Shandong University of Politics Science and Law, Jinan 250014, China*

[2] *College of Physics and Electronics, Shandong Normal University, Jinan 250014, China*

[*] *Corresponding author: chengchuanfu@sdnu.edu.cn*

Received September 22, 2011; accepted December 12, 2011; posted online March 15, 2012

A practicable experimental method for measuring scattering on rough surfaces is reported. The scattered patterns are captured on a screen composed of two pieces of ground glass and then imaged using a charge-coupled device. The scattered intensity profiles are extracted by converting the patterns in real space into the wave vector space. Isotropic and anisotropic samples of the rough backsides of silicon wafer are investigated respectively, and their intensity profiles are measured. The profiles of the anisotropic sample are obtained by reading the pixels on the specific orientation curves. The parameters of the samples are extracted using angle-resolved light-scattering schemes and theories. The results well agree with measurements obtained using an atomic force microscope.

OCIS codes: 290.5880, 120.5820, 120.6650.

doi: 10.3788/COL201210.052901.

Light scattering from random rough surfaces has been a long-standing research subject. Since the 1990s, significant advancements in the characterization of rough fractal surfaces by light scattering have been achieved[1−4]. Fundamentally, Sinha *et al.* proposed a classical scattering model for rough self-affine fractal surfaces[5], and Yang *et al.* constructed mathematical relations of the half-width of the scattered intensity profiles with the parameters of rough self-affine fractal surfaces[6]. Eventually, more systematical theories and angle-resolved experimental schemes were developed for the extraction of the parameters of rough self-affine surfaces from the scattered intensity profiles[7]. Meanwhile, in the area of light scattering, scattering models and experimental methods were continuously developed to deal with the complexity of diverse practical problems[8,9]. Nowadays, light scattering has become one of the most important means of detecting surface characteristics and nanostructures. In the experimental aspect, delicate devices have been implemented for the measurement of scattered intensity profiles. One of the most frequently employed is the scatterometer designed by Shen *et al.*[10], which can be used to adjust scattering angles conveniently. Most works use a single detector to capture scattered light[7,10,11]. Thus, the movement of the detector makes the acquisition of an intensity profile time consuming. Another alternative device is the linear detector array[7], in which a scattered intensity profile is taken along a straight line on the measurement plane. However, for some experimental methods, light intensity has to be measured along a specific curve[10,12]. In addition, the limited extending range of the linear detector array can receive only a small part of the intensity profiles and thus induce errors in surface parameter extraction.

In this letter, we propose an experimental method for the extraction of intensity profiles by imaging the scattered pattern with a charge-coupled device (CCD) camera. The scattered pattern is first captured by a screen composed of two pieces of ground glass and then imaged by the CCD. The light intensity profiles are obtained by reading the pixels of the scattered pattern images along line segments or specific curves and are converted into profiles in the wave vector space. The parameters of the sample surface are extracted from the light intensity profiles. Both the experimental operation and data processing are time saving and convenient. The method is demonstrated by practically investigating two samples, one being isotropic and the other anisotropic. The parameters of the two samples are obtained and compared with measurements obtained by an atomic force microscope (AFM).

The experimental setup is shown in Fig. 1(a). The optical path lies in a horizontal plane. A light beam from a He–Ne laser, which has a wavelength of 632.8 nm, is reflected by mirror M. Two polarizers, namely, P1 and P2, are used to adjust the intensity of the incident light beam. The polarization of the incident beam is kept vertical via P2. Pinhole H, which has a diameter of approximately 4 mm, is used to filter out stray light. Rough sample S is mounted on a rotational stage, with which the orientation of the sample plane and the incident angle are changed. Lens L1, with a focal length of 18 cm, is placed in front of the sample to form the Fraunhofer diffraction geometry. A screen is used to receive the scattered pattern on the focal plane of L1. The screen is composed of two pieces of ground glass, G1 and G2, and a piece of white paper clamped between them. Here, G1 and G2, having sufficient roughness (ground with 240# Al_2O_3 powder), and the paper piece are used so that the

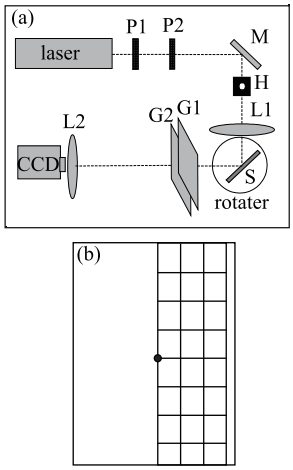

Fig. 1. (a) Experimental setup for the light-scattering measurement by imaging the scattered pattern using a CCD; (b) paper labeled with square grids.

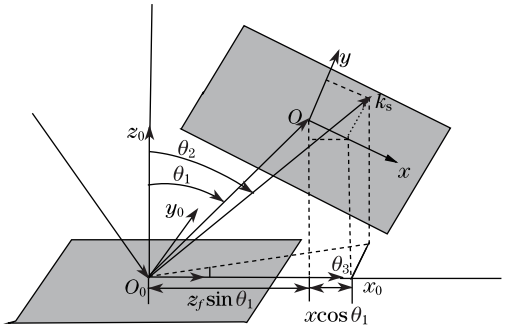

Fig. 2. Schematic diagram of the light-scattering geometry.

scattered pattern is uniformly imaged by lens L2 onto the CCD pixel plane. The paper piece is labeled with square grids of 3 cm side length and a small circular point, as shown in Fig. 1(b), for position determination purposes. The distance z_f between the screen and the sample can be measured directly for the calculation of the wave vectors in data processing. The focal length of L2 is 5 cm, and the distance between lens L2 and the screen is adjusted to ensure that the whole scattered pattern is imaged within the range of the CCD (Roper Cascade 1 k, 16 b dynamic range, –30 °C, 1 004×1 002 pixels, and 8×8 μm pixel size).

For the theoretical analysis, the scattering geometry in the experimental setup is schematically shown in Fig. 2. The sample S lies in the $O_0x_0y_0$ plane. The incident plane is $O_0x_0z_0$, and the incident angle is θ_1. The angle of reflection is θ_1 but is in the opposite side of the z_0 axis. θ_2 and θ_3 are the scattering angles, and the azimuthal angle k_S is the scattering wave vector. The wave vector is $\boldsymbol{k} = \boldsymbol{k}_S - \boldsymbol{k}_0$, where $\boldsymbol{k}_0$ is the wave vector of the incident beam. According to the Kirchhoff theory of diffraction, the simplified and approximated scattered light wave $U(k_\perp, \boldsymbol{k}_{||})$ from the rough surface sample is written as[7]

$$U(k_\perp, \boldsymbol{k}_{||}) = \int_A \exp\{-\mathrm{i}[\boldsymbol{k}_{||} \cdot \boldsymbol{r}_0 + k_\perp h(\boldsymbol{r}_0)]\}\mathrm{d}^2\boldsymbol{r}_0, \quad (1)$$

where A represents the integral area and $h(\boldsymbol{r}_0)$ is the height distribution of the rough surface. $\boldsymbol{k}_{||}$ and $k_\perp$ are the $\boldsymbol{k}$ components parallel and perpendicular to the plane of sample S, respectively, $k_\perp$ which are expressed as

$$\boldsymbol{k}_{||} = k_0(\sin\theta_2\cos\theta_3 - \sin\theta_1)\hat{\boldsymbol{x}}_0 + k_0\sin\theta_2\sin\theta_3\hat{\boldsymbol{y}}_0, \quad (2)$$

$$k_\perp = k_0(\cos\theta_1 + \cos\theta_2). \quad (3)$$

For rough surfaces with Gaussian height probability distributions, the scattered intensity may be simplified from Eq. (1) as

$$I(k_\perp, \boldsymbol{k}_{||}) = \langle U(k_\perp, \boldsymbol{k}_{||})U^*(k_\perp, \boldsymbol{k}_{||})\rangle = c^2 \int_{-\infty}^{\infty} \exp[-k_\perp^2 H(\rho)]\exp[-\mathrm{i}\boldsymbol{k}_{||} \cdot \rho]\mathrm{d}^2\rho, \quad (4)$$

where $H(\boldsymbol{\rho}) = \langle[h(\boldsymbol{r}_0 + \boldsymbol{\rho}) - h(\boldsymbol{r}_0)]^2\rangle$ is the height–height correlation function of the rough surface and c is a constant. For isotropic rough self-affine fractal surfaces, $H(\boldsymbol{\rho})$ may be expressed by the phenomenological function $H(\rho) = 2w^2\{1 - \exp[-(\rho/\xi)^{2\alpha}]\}$ with $\rho = |\boldsymbol{\rho}|$[5]. Here, w is the root-mean-square (RMS) roughness, ξ is the correlation length of the surface, and α is the roughness exponent related to the surface fractal dimension D_f, which is expressed as $\alpha = d - D_f$, with $0 \leqslant \alpha \leqslant 1$ and d being the embedded dimension.

In the angle-resolved scattering scheme, the scattering profiles are taken from different incident angles, and the variation of the profiles and the specular reflection part with the change in $k_\perp$ are utilized. After simple calculations, Eq. (4) becomes

$$I(k_\perp, \boldsymbol{k}_{||}) = I_\delta(k_\perp)\delta(\boldsymbol{k}_{||}) + I_{\mathrm{diff}}(k_\perp, \boldsymbol{k}_{||}), \quad (5)$$

with the reflection and diffused parts denoted as $I_\delta(k_\perp) = c^2\exp(-k_\perp^2 w^2)$ and

$$I_{\mathrm{diff}}(k_\perp, \boldsymbol{k}_{||}) = c^2 \int_{-\infty}^{+\infty} \{\exp[-k_\perp^2 H(\boldsymbol{\rho})/2] - \exp[-k_\perp^2 w^2]\} \cdot \exp(-\mathrm{i}\boldsymbol{k}_{||} \cdot \rho)\mathrm{d}^2\rho. \quad (6)$$

Here, the expression for $I_\delta(k_\perp)$ can be deduced by averaging the scattered light field $U(k_\perp, \boldsymbol{k}_{||})$ and using the Gaussian probability density function of surface height $h(\boldsymbol{r}_0)$, as shown by Liu *et al.*[13]. From Eqs. (5) and (6), the ratio R_δ of the integrated intensity of the specular reflection to the total integrated intensity is expressed as $R_\delta = I_\delta/I = \exp(-k_\perp^2 w^2)$. Then, this ratio can be used to extract the roughness w of the samples. Although the analytical expression of the transform of Eq. (6) is unattainable, approximations may be made and the half-width W_p of the diffused part of the profile may be obtained in the limit cases[14]

$$W_\mathrm{p} = \begin{cases} 2/\xi, & k_\perp^2 w^2 << 1 \\ 2/(k_\perp^{-1/\alpha} w^{-1/\alpha}\xi), & k_\perp^2 w^2 >> 1 \end{cases}. \quad (7)$$

With this equation and the angle-resolved experimental setup, the value of the correlation length can be obtained using $\xi = 2/W_\mathrm{p}$ from the half-width of the profile provided that $k_\perp^2 w^2 << 1$. The roughness exponent α can be extracted from the variation of the half-widths W_p of the profile versus $k_\perp$, with $\ln W_\mathrm{p} \propto (1/\alpha)\ln k_\perp$, by using the other limit case, i.e., $k_\perp^2 w^2 >> 1$, and by measuring

the diffused profiles at different angles of incidence.

All of the above equations are provided in the wave vector space and in the discussions, and the variation of $k_\perp$ in detecting a single intensity profile is assumed to be insignificant. The measurements of the scattered intensities are conducted in real space. Thus, the wave vector components $\boldsymbol{k}_{||}$ and $k_\perp$ first have to be transformed into the real space coordinates $O_0 - x_0y_0z_0$ and Oxy. The receiving screen in Fig. 2 is perpendicular to the direction of reflection and lies in the Oxy plane. Therefore, from the geometrical relation, a point (x, y) on the Oxy plane may be expressed in the $O_0 - x_0y_0z_0$ coordinates using

$$\begin{cases} z_0 = z_f \cos\theta_1 - x\sin\theta_1 \\ x_0 = z_f \sin\theta_1 + x\cos\theta_1 \\ y_0 = y \end{cases} . \tag{8}$$

As presented in Fig. 2, the relation between the angles and the coordinates can be denoted as

$$\begin{cases} \sin\theta_2 = \dfrac{\sqrt{x_0^2 + y_0^2}}{\sqrt{x_0^2 + y_0^2 + z_0^2}} \\ \sin\theta_3 = \dfrac{y_0}{\sqrt{x_0^2 + y_0^2}} \\ \cos\theta_3 = \dfrac{x_0}{\sqrt{x_0^2 + y_0^2}} \end{cases} . \tag{9}$$

With Eqs. (8) and (9), as well as Eqs. (2) and (3), the scattered intensity distributions on the receiving screen can be converted into intensity profiles with variables $\boldsymbol{k}_{||}$ and $k_\perp$. Afterward, the surface parameters may be extracted.

Next, an experiment on the two samples of the backsides of commercial silicon wafers is conducted. One sample is isotropic, and the other is anisotropic. First, the samples are measured using an AFM, and their morphological images are shown in Figs. 3(a) and (b), respectively. Four images from different areas of each sample were taken to obtain average data and hence avoid errors due to the limited scan range. For the AFM measurement, the anisotropic sample was carefully adjusted so that sides of the small square-pit-like structures on the surface are parallel to the sides of the images. The roughness values (w) of the samples are calculated using the height data from their AFM images and are given in Table 1. The averaged height–height correlation function $H(\rho)$ of the images is calculated to determine the lateral correlation length ξ and roughness exponent α from the AFM images. The roughness exponent α is obtained by linearly fitting the height–height correlation function curve with the $\rho << \xi$ region, where $\ln[H(\rho)] \propto 2\alpha \ln(\rho)$. On the other hand, the values of ξ are obtained by fitting the numerical function $H(\rho)$ with the phenomenological function of the height–height correlation for the self-affine fractal model.

In the light-scattering measurement, each image of the scattered patterns at a certain angle of incidence is sampled 100 times with the CCD accumulations to reduce electric noise. In addition, four images of the pattern are taken at different positions of the same sample to obtain averaged data and eliminate speckles. The disturbance of the speckle effect on the scattered profiles can be decreased by using an imaging lens with a large relative aperture ($f1.8$) to produce speckles with extremely small average sizes such that a CCD pixel can cover several (approximately over 10) speckle grains. Then, the effect of speckles is physically averaged by the CCD detection. The scattered patterns of each sample are taken at incident angles from 40° to 80°, with increments of 5°, and at 83°. Some of scattered pattern images for the two samples are shown in Figs. 4(a) and (b).

The differences among the scattered patterns of the isotropic and anisotropic samples and the evolutions of the patterns with the angle of incidence can be clearly seen in Fig. 4. For the isotropic sample, the distribution of the intensity pattern is nearly round and uniform at a smaller incident angle. As the angle is increased, the pattern contracts, more evidently in the vertical direction, and appears to be oblate. For the anisotropic sample, secondary peaks exist on the four sides of the main peak. As the incident angle is increased, the lower and upper

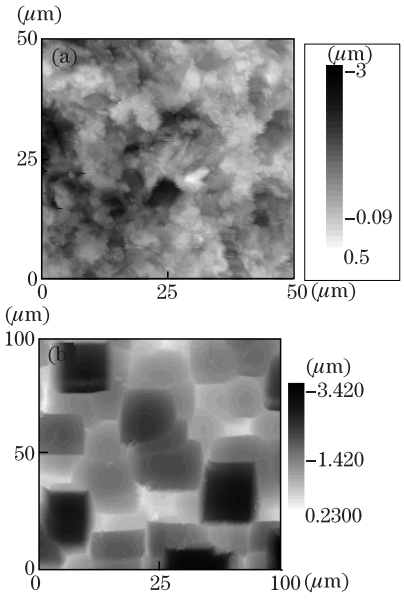

Fig. 3. AFM images of the two kinds of rough surface samples. (a) Isotropic sample with 50×50 (μm) scan area and (b) anisotropic sample with 100×100 (μm) scan area.

Table 1. Parameters of the two Samples Obtained Using Light Scattering and AFM

Sample	w (μm)		ξ (μm)		α	
	AFM	LS	AFM	LS	AFM	LS
Isotropic	0.47±0.03	0.34	4.16±0.17	5.21±0.22	0.68±0.02	0.70±0.02
Anisotropic	0.74±0.10	0.63	12.07±0.10	11.36±0.46	0.73±0.01	0.77±0.09

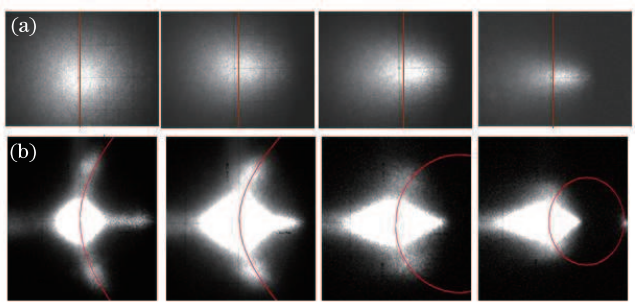

Fig. 4. Scattering intensity maps at different angles of incidence for the (a) isotropic and (b) anisotropic samples. The incident angles from left to right are 40°, 55°, 70°, and 75°, respectively.

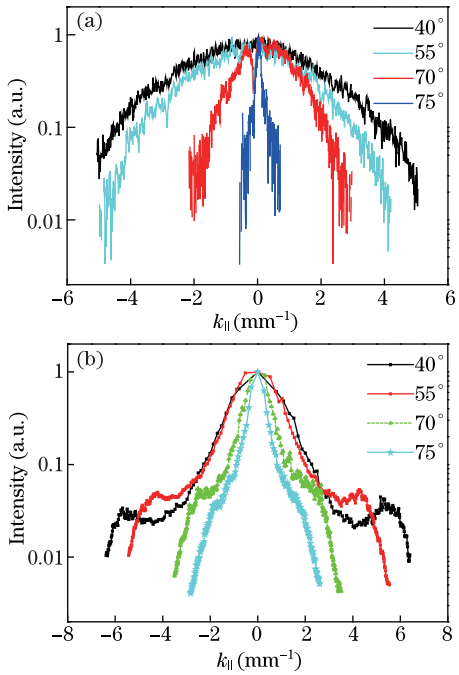

Fig. 5. Diffused intensity profiles at the different incidence angles for the (a) isotropic and (b) anisotropic samples.

secondary peaks contract toward the central main peak and the centers of the peaks form a curve.

The scattered intensity profiles of the isotropic sample are extracted from the intensity patterns by reading the data in the pixels along the red vertical lines, as shown in Fig. 4(a). Along each line segment, the coordinate y in Oxy varies as in Fig. 2, whereas θ_2 changes insignificantly. Based on Eqs. (2), (3), (8), and (9), $k_{||}$ therefore changes with y, and $k_\perp$ can be approximately regarded as a constant. Then, with the coordinates converted into $k_{||}$, the intensity profile $I(k_\perp, k_{||})$ at an incident angle is obtained. Figure 5(a) presents the typical normalized profile curves at incident angles of 40°, 55°, 70°, and 75°, respectively. Then, the surface parameters are extracted from all profiles. The profile at 75° is used to calculate the ratio R_δ of the specular reflection intensity to the total integrated intensity of the profile, and the roughness value w of the sample is obtained as 0.34 μm (Table 1). The lateral correlation length of the sample is obtained from the half-width $W_{\rm p}$ of the profile at 75°, with a value of ξ=5.21±0.22 μm. The roughness exponent α is extracted using the half-widths of the profiles at 50°, 55°, 60°, and 65° to obtain the variation of $W_{\rm p}$ versus $k_\perp$. Subsequently, α is obtained as $\alpha = 0.70 \pm 0.02$ using Eq. (7).

The extraction of the intensity profiles from the patterns is more complicated for the anistropic sample. In the light-scattering experiment, the orientations of the sample need to be carefully adjusted such that the sides of the square pits on the surface shown in Fig. 3(b) are parallel to the x_0 and y_0 directions, as shown in Fig. 2. The orientations can be adjusted by ensuring that the patterns in Fig. 4(b) are symmetrical with respect to the horizontal direction. Notably, in Eq. (4), the phase factor in the Fourier transform is $\exp[-{\rm i}(k_{||x}x_0 + k_{||y}y_0)$, and the sample has the same statistical properties along the x_0 and y_0 directions. Moreover, the transform may be simplified with respect to $k_{||y}$ by assuming that $k_{||x} = 0$. From Eq. (2), the condition of $k_{||x} = 0$ is written as

$$k_0(\sin\theta_2\cos\theta_3 - \sin\theta_1) = 0. \tag{10}$$

After substituting Eqs. (8) and (9) into (10), the relation between x and y can be obtained as

$$y^2\sin^2\theta_1 = x^2\cos 2\theta_1 + xz_f\sin 2\theta_1. \tag{11}$$

Interestingly, $k_{||x} = 0$ transforms into a curve expressed by the above equation in the Oxy plane. This curve is called the orientation curve and varies with the incident angle and the scattering distance z_f. The profiles at different incident angles are taken by reading the intensity data in the pixels along the orientation curves, as shown in Fig. 4(b). Figure 5(b) shows the normalized profile $I(k_\perp, k_{||})$ curves at incident angles of 40°, 55°, 70°, and 75°, respectively. The parameters of the sample can be obtained using the aforementioned method. In the extraction of the roughness exponent, the ratio R_δ is calculated with the profile at 83° to obtain w=0.63 μm. The lateral correlation length is extracted from the profile at 83° as ξ=11.36±0.46 μm. The roughness exponent is obtained as $\alpha = 0.77 \pm 0.09$ from the half-widths of the profiles at 45°, 50°, 55°, and 60°. Table 1 shows the comparison between these parameters and the AFM measurements.

Table 1 shows that the results obtained by the light-scattering method roughly conform with the AFM measurements. In general, the roughness values obtained by light scattering are smaller than those obtained by the AFM. Such discrepancy may be due to the deviation in height as the AFM measurements have a relative tilt height background. Other possible reasons for the discrepancy in surface parameters may be factors such as the approximations taken in the theoretical analysis, the systematic errors in the experiments, and the conversion of coordinates into the wave vector space.

In the experiment, the central δ peak should be measurable, which would limit the roughness of the samples in a suitable range. Practical experience shows that a roughness value from 0.05 to 1.20 μm is sufficiently accurate. The lateral correlation length ξ determines the half-width $W_{\rm p}$ of the intensity profile in the case of $k_\perp^2 w^2 << 1$. Thus, the feasibility of resolving the whole scattered profile determines the measurable range. According to experience, this range is approximately from 2.0 to 15.0

μm. In addition, several assumptions and approximations were used in the theoretical derivations. Firstly, the Kirchhoff theory of diffraction under the condition of Eq. (1) is widely used in literature and is shown to be sufficiently accurate. Secondly, for the surface model, a self-affine fractal rough surface with Gaussian distribution was used, and based on which, Eq. (4) and the $H(\rho)$ expression were obtained. Furthermore, the AFM data of the samples were analyzed, and the results showed good consistency with those of the model. For the extraction of roughness exponent α, the condition $k_{\perp}^2 w^2 >> 1$ in Eq. (7) was used, which may be evaluated by the linear proportion of $W_{\rm p}$ versus $\ln k_{\perp}$ in the large $k_{\perp}$ region, and accurate results were obtained.

In conclusion, we present a convenient and practicable method for the light-scattering measurement of rough surface samples, which is done by imaging the scattering patterns and using light-scattering theories. Aside from providing clear images for the study of the scattering properties of the samples, the experimental setup also reduce the difficulty in the acquisition of scattering intensity data. The convenience in reading the data in any pixels of the images facilitated the analysis of the scattering of the anisotropic sample by taking the profiles along the specific orientation curves. The experimental results indicate that the setup and method proposed in this letter are effective and convenient for the light-scattering measurement of random rough surfaces.

The work was supported by the National Natural Science Foundation of China (Nos. 10974122 and 10874105) and the Shandong Provincial Project for Scientific and Technological Development of China (Nos. ZR2009AM025 and BS2009SF020).

References

1. D. Liu, Y. Yang, L. Wang, Y. Zhuo, C. Lu, L. Yang, and R. Li, Opt. Commun. **278,** 240 (2007).
2. W. Choi, C.-C. Yu, C. Fang-Yen, K. Badizadegan, R. R. Dasari, and M. S. Feld, Opt. Lett. **33,** 14 (2008).
3. Z. Wei, X. Long, and K. Yang, Chin. Opt. Lett. **8,** 2 (2010).
4. F. Bordi, C. Cametti, A. DiBiasio, M. Angeletti, and L. Sparapani, Bioelectrochemistry **52,** 213 (2000).
5. S. K. Sinha, E. B. Sirata, S. Garoff, and H. B. Stanley, Phys. Rev. B **38,** 2297 (1988).
6. H. N. Yang, T. M. Lu, and G. C. Wang, Phys. Rev. B **47,** 3911 (1993)
7. Y. P. Zhao, G. C. Wang, and T. M. Lu, *Characterization of Amorphous and Crystalline Rough Surface*: *Principles and Applications* (Troy, New York, 2001).
8. T. M. Elfouhaily and C.-A. Gu'erin, Waves Random Media 14:4, R1-R40 (2004).
9. R. Li Voti, G. L. Leahu, S. Gaetani, C. Sibilia, V. Violante, E. Castagna, and M. Bertolotti, J. Opt. Soc. Am. B **26,** 8 (2009).
10. Y. J. Shen, Q. Z. Zhu, and Z. M. Zhang, Rev. Scientific Instruments **74,** 4885 (2003)
11. M.-J. Kim, J. C. Dainty, A. T. Friberg, and A. J. Sant, J. Opt. Soc. Am. A **7,** 4 (1990).
12. T. Karabacak, Y. Zhao, M. Stowe, B. Quayle, G.-C. Wang, and T.-M. Lu, Appl. Opt. **40,** 31 (2001).
13. D. Liu, D. Qi, and C. Cheng, Chinese J. Lasers B **9,** 3 (2000).
14. C. Cheng, C. Liu, S. Teng, N. Zhang, and M. Liu, Phys. Rev. E **65,** 061104 (2002)